arXiv:nucl-th/0203028v1 13 Mar 2002

Investigation of the high momentum component of nuclear wave function using hard quasielastic A(p,2p)X reactions.

I. Yaron, J. Alster, L. Frankfurt, E. Piasetzky
School of Physics and Astronomy, Sackler Faculty of Exact Sciences, Tel Aviv University, Ramat Aviv 69978, Israel

M. Sargsian
Department of Physics, Florida International University, Miami, FL 33199, U.S.A

M. Strikman
Department of Physics, Pennsylvania State University, University Park, PA 16802, U.S.A

February 8, 2008

Abstract

We present theoretical analysis of the first data on the high energy and momentum transfer (hard) quasielastic $C(p,2p)X$ reactions. The cross section of hard $A(p,2p)X$ reaction is calculated within the light-cone impulse approximation based on two-nucleon correlation model for the high-momentum component of the nuclear wave function. The nuclear effects due to modification of the bound nucleon structure, soft nucleon-nucleon reinteraction in the initial and final states of the reaction with and without color coherence have been considered. The calculations including these nuclear effects show that the distribution of the bound proton light-cone momentum fraction (α) shifts towards small values ($\alpha < 1$), effect which was previously derived only within plane wave impulse approximation. This shift is very sensitive to the strength of the short range correlations in nuclei. Also calculated is an excess of the total longitudinal momentum of outgoing protons. The calculations are compared with data on the $C(p,2p)X$ reaction obtained from the EVA/AGS experiment at Brookhaven National Laboratory. These data show α-shift in agreement with the calculations. The comparison allows also to single out the contribution from short-range nucleon correlations. The obtained strength of the correlations is in agreement with the values previously obtained from electroproduction reactions on nuclei.

I. INTRODUCTION

One of the important signatures of quark-gluon structure in nucleon-nucleon interaction at short distances is the observed strong energy dependence ($\sim s^{-10}$) of the wide angle pp elastic differential cross section at $s \geq 12\ GeV^2$, where s is the square of the pp c.m. energy. Despite the ongoing debate on the validity of perturbative QCD in this energy region [1–3] or the debate on the relevance of a particular mechanism of subnucleon interaction (i.e. quark-interchange [4–6], three-gluon exchange [7,8], reggeon-type contribution [9]), it is commonly accepted that the power-law s- dependence of the elastic cross section signals the onset of the hard dynamics of the quark-gluon interaction.

In this paper we address the question of what happens when wide angle pp scattering takes place inside the nucleus, i.e. the incident proton is scattered off a bound proton. If this reaction would have the same $\sim s^{-10}$ energy dependence as that of the cross section of free pp scattering, one may expect that the incoming proton will favor to scatter off a bound proton with larger initial momentum aligned to the direction of the incoming proton [10,11]. This kinematic condition corresponds to pp scattering with smaller s and therefore larger scattering cross section. Thus, if nuclear effects will not alter the genuine s-dependence of the pp cross section, the high momentum transfer $p + A \to p + p + X$ reaction would select preferably the high momentum components of the nuclear wave function.

Due to the short-range nature of the strong interaction, the high internal momentum in the nucleus will be generated mainly by short-range NN correlations. Therefore, at sufficiently high energies and high momentum transfers one expects to probe the short-range properties of the nucleus. In Ref. [10,11] within a plane wave impulse approximation (PWIA) the authors calculated the cross section of high momentum transfer $A(p, 2p)X$ reactions and observed a strong sensitivity to the high momentum component of the nuclear wave function.

Motivated by the recent measurements of high-momentum transfer pA reactions at Brookhaven National Laboratory (BNL) [12] we carried out a detailed analysis of the high-momentum transfer $A(p, 2p)X$ reaction investigating specifically the competing nuclear effects, not discussed previously. These effects may obscure the observed sensitivity shown within PWIA [11]. Our main goal is to see whether these reactions probe short range correlations (SRC) and their sensitivity to the dynamical structure of these correlations.

The structure of the paper is as follows. In Chapter 2 we outline the basic theoretical framework for the calculation of the high-energy wide angle quasielastic $A(p, 2p)X$ reaction. We also discuss the nuclear effects which can compete with the expected signatures of the scattering from SRC. In Chapter 3 we present the predictions of the model presented in the Chapter 2. Chapter 4 describes briefly the EVA experiment at BNL. The calculations are compared with the data obtained in this experiment in chapter 5. In chapter 6 we summarize the results of our study.

II. THE BASIC THEORETICAL FRAMEWORK

In quasi-elastic (QE) scattering a projectile is elastically scattered from a single bound "target" nucleon in the nucleus while the rest of the nucleus acts as a spectator. A schematic presentation of (p,2p) QE scattering is given in Fig 1.

FIGURES

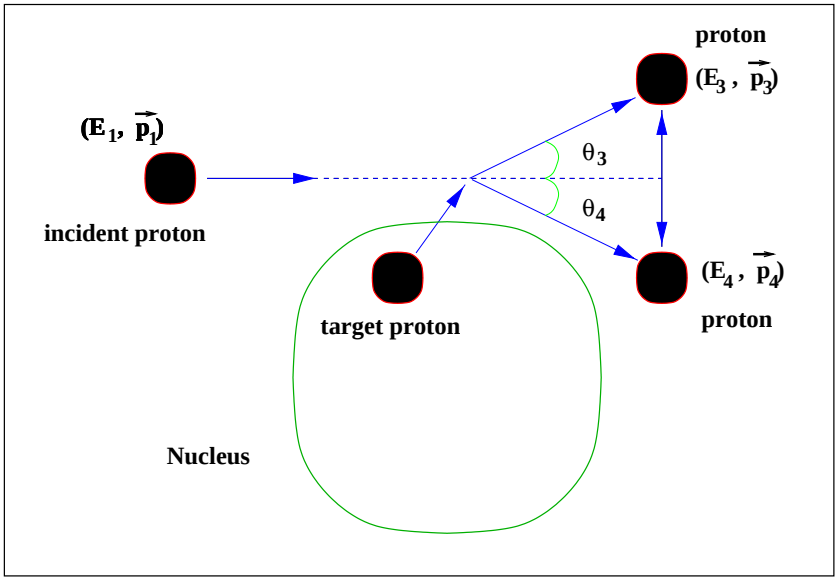

FIG. 1. The kinematics for quasi-elastic $A(p,2p)X$ scattering.

A. Kinematics

$p_A = (E_A, \vec{p_A})$, $p_1 = (E_1, \vec{p_1})$, $p_3 = (E_3, \vec{p_3})$, $p_4 = (E_4, \vec{p_4})$, $p_R = (E_R, \vec{p_R})$ - are the four - momenta of the target nucleus, the incoming proton, the scattered proton, the ejected proton and the recoil nucleus, respectively. For simplicity we did not show in the Figure 1 p_A and p_R. Using the variables defined in the figure the Mandelstam variables are:

$$s = (p_3 + p_4)^2 \ ; \ t = (p_1 - p_3)^2. \tag{1}$$

The high-momentum transfer primary process in the $A(p,2p)X$ quasi-elastic reaction is the hard pp elastic scattering. Since the general predictions are based on the implication of the strong s-dependence ($\sim 1/s^{10}$) of hard elastic pp cross section we will limit our calculations to high energy and high momentum transfer kinematics were the $1/s^{10}$-dependence is observed experimentally for pp scattering off hydrogen target. Thus, our calculations are limited to $s \gtrsim 12\ GeV^2$ and $\theta_{cm} \sim 90^0$.

The missing energy (E_m) for the $A(p,2p)X$ reaction is given by $E_m = E_1 + E_A - E_3 - E_4 - E_{A-1}$. The available high energy $A(p,2p)X$ data have a missing energy resolution of about 240 Mev [12]. Therefore, the calculations which we compare with the data are integrated over a wide range of missing energy. This integration simplifies the calculations as will be discussed below.

B. Plane Wave Impulse Approximation

A clear interpretation of the quasi-elastic measurements is possible in Plane Wave Impulse Approximation (PWIA). Within this approximation it is possible to separate nuclear properties from the reaction mechanism.

In a high energy scattering the reaction evolves near the light cone $\tau = t - z \sim 1/(E + p_z) \ll t + z$, where z is the direction of the incident proton and E, p_z are the energy and leading longitudinal momentum of the high energy particles involved in the scattering. Thus it is natural to describe the reaction in the light cone reference frame (similar to high energy deep-inelastic scattering from hydrogen target see e.g. [13]).

Within the light cone plane wave impulse approximation the cross section of the quasielastic $A(p, 2p)X$ reaction can be represented as a convolution of the elementary elastic pp scattering cross section off bound nucleon and the four - dimensional Light Cone Spectral function [10]:

$$\frac{d^6\sigma}{(d^3p_3/2E_3)(d^3p_4/2E_4)} = \sum_Z \frac{1}{4j_{pA}} \frac{|M_{pp}|^2}{(2\pi)^2} \cdot \frac{P_A(\alpha, p_t^2, p_{R+})}{\alpha^2} = \\ = \sum_Z \frac{2}{\pi} \sqrt{s^2 - 4m^2 s} \frac{d\sigma}{dt}^{pp}(s,t) \cdot \frac{P_A(\alpha, p_t^2, p_{R+})}{A \cdot \alpha} \tag{2}$$

where

$$p_2 = p_3 + p_4 - p_1 \ ; \ p_t = p_3^t + p_4^t \\ \alpha = \alpha_4 + \alpha_3 - \alpha_1 \ ; \ \alpha_i = A\frac{p_{i-}}{P_{A-}} \equiv A\frac{E_i - p_i^z}{E_A - P_A^z}. \tag{3}$$

The superscript "t" and "z" denote the transverse (x, y) and longitudinal directions with respect to incoming proton momentum $\vec{p}_1$. The " $+$ " and " $-$ " indices denote the energy and longitudinal components of four - momenta in the light cone reference frame [1]. The variable α defined in Eq.(3) describes the light cone momentum fraction of nucleus carried out by target nucleon, normalized in such a way that a nucleon at rest has $\alpha = 1$. The j_{pA} - is the invariant flux with respect to the nucleus, the M_{pp} and $\frac{d\sigma}{dt}^{pp}$ - are the invariant amplitude and cross section for elastic pp scattering.

The Light Cone spectral function represents the probability to find the target nucleon with the light cone momenta (α, p_t) times the probability that the residual nuclear system has a momentum component $p_{R+} = E_R + p_R^z$. The Spectral function is normalized as follows [10]:

$$\int \frac{p_{A-}}{2A} P_A(\alpha, p_t^2, p_{R+}) \frac{d\alpha}{\alpha} d^2p_t dp_{R+} = A. \tag{4}$$

---

[1] Since z directions is chosen as the direction of incoming proton momentum, the "-" component corresponds to the light cone longitudinal momentum, which is conserved at the scattering vertices.

C. The Light Cone Spectral Function

The integration over a wide range of the missing energy allows us to use the following approximations for the spectral function:

For target proton momenta below the Fermi sea level ($p_2 < p_{Ferm} \sim 250 MeV/c$) we use the nonrelativistic limit of the light cone spectral function [14,10]:

$$P_A(\alpha, p_t^2, p_{R+}) \approx \frac{1}{2} n(p_2) \cdot \delta(p_{R+} - (\sqrt{M_{A-1}^2 + p_2^2} - p_2^z)), \tag{5}$$

where $\alpha \approx 1 - p_2^z/m$ and $\vec{p}_2 = \vec{p}_3 + \vec{p}_4 - \vec{p}_1$ are the missing momentum components of the reaction. $n(p)$ is the momentum distribution of nucleons calculated within the mean field approximation.

For the momentum range of ($p_{Ferm} < p_2 < 0.7\ GeV/c$) we assume the dominance of the two nucleon short-range correlations which allows to model the spectral function as follows [10,15]:

$$P_A(\alpha, p_t^2, p_{R+}) \approx \int \frac{A^2}{2p_{A-}} a_2(A) \cdot \rho_2^n \left(\frac{2\alpha}{(A-\beta)}, (\vec{p}_t + \frac{\alpha}{(A-\beta)} \vec{p}_{(A-2)t})^2 \right) \cdot \rho_{A-2}(\beta, p_{(A-2)t}^2) \cdot$$
$$\delta \left(p_{R+} - \frac{m^2 + (\vec{p}_{(A-2)t} + \vec{p}_t)^2}{m(A-\alpha-\beta)} - \frac{M_{A-2}^2 + p_{(A-2)t}^2}{m\beta} \right) \frac{d\beta}{\beta} d^2 p_{(A-2)}^t, \tag{6}$$

where $(\beta, p_{(A-2)t}^2)$ and ρ_{A-2} are the light cone momentum and the density matrix of the recoiling $(A-2)$ system. The parameter $a_2(A)$ is the probability of finding two-nucleon correlations in the nucleus A and ρ_2^n is the density matrix of the correlated pair which we set equal to the Light Cone density matrix of the deuteron [14]:

$$\rho_2^n(\alpha, p_t^2) = \frac{\Psi_D^2(k)}{2-\alpha} \sqrt{m^2 + k^2}\ ;\ k = \sqrt{\frac{m^2 + p_t^2}{\alpha(2-\alpha)} - m^2}\ ;\ (0 < \alpha < 2). \tag{7}$$

Note that the factorization of the nuclear density matrix to the correlation and $(A-2)$ density matrices is specific for the short-range two-nucleon correlation approximation. In this approximation it is assumed that the singular character of NN potential at short distances (existence of repulsive core) defines the main structure of the nucleon momentum distribution in SRC and it is less affected by the collective interaction with the $A-2$ nuclear system. Notice that the expression in Eq.(7) is the light cone analog of the approximated spectral function used in Ref. [16], where the validity of two-nucleon correlation approximation is demonstrated comparing the prediction of nonrelativistic analogue of Eq.(6) with the exact calculations of spectral function of ^3He nucleus and infinite nuclear matter.

To obtain the density matrix of the recoiling $(A-2)$ system, additional physical assumptions are required. However the fact that we are interested in the cross section integrated over a wide range of the missing energy allows us to simplify the Eq.(6) by neglecting the momentum of the recoiling $(A-2)$ system (SRC at rest approximation):

$$\rho_{A-2}(\beta, p_{(A-2)t}^2) = (A-2) \cdot \delta(A-2-\beta) \cdot \delta(p_{(A-2)t}^2). \tag{8}$$

Inserting Eq.(8) into Eq.(6) one obtains the following expression for the light cone spectral function in the high missing momentum range:

$$P_A(\alpha, p_t^2, p_{R+}) \approx \frac{A^2}{2p_{A-}} a_2(A) \cdot \rho_2^n(\alpha, p_t^2) \cdot \delta(p_{R+} - \frac{m^2 + p_t^2}{m(2-\alpha)} - M_{A-2}). \quad (9)$$

It is worth noting that the above approximation is justified based on the observation of Ref. [16] that it correctly predicts the position of the maximum in the missing energy distribution at fixed values of missing momenta. Therefore, in regime in which the integration over the wide range of missing energies is allowed, Eq.(9) represents a valid approximation of nuclear spectral function at the SRC domain. The same model was also used to describe the inclusive nucleon and pion production in kinematics forbidden for scattering off a free nucleon [10,14] and electroproduction [14,15] reactions from nuclei at $x > 1$ and $Q^2 \geq 1\ GeV^2$.

D. Proton-Proton Elastic Scattering Cross Section

The next quantity which is needed to calculate the quasielastic $A(p, 2p)X$ cross section in Eq.(2) is the differential cross section of pp elastic scattering. For $s \geq 12\ GeV^2$ we use the phenomenological parameterization of the free pp elastic cross section. We assumed a combination of s-parameterization at 90^0 presented in Ref. [37] and $\theta_{c.m.}$-parameterization in the form suggested in Ref [18]:

$$\frac{d\sigma}{dt}^{pp} = 45.0 \frac{\mu b}{sr GeV^2} \cdot \left(\frac{10}{s}\right)^{10} \cdot (1 - \cos\theta_{c.m.})^{-4\gamma} \cdot$$
$$\left[1 + \rho_1 \sqrt{\frac{s}{GeV^2}} \cdot \cos\phi(s) + \frac{\rho_1^2}{4} \frac{s}{GeV^2}\right] \cdot F(s, \theta_{c.m.}) \quad (10)$$

where $\rho_1 = 0.08$, $\gamma = 1.6$ and $\phi(s) = \frac{\pi}{0.06} \ln(\ln[s/(0.01 GeV^2)])^{-2}$. The function $F(s, \theta_{c.m.})$ is used for further adjustment of the phenomenologically motivated parameterization to the experimental data at $60^0 \leq \theta_{c.m.} \leq 90^0$ [19].

E. Calculation of the α-dependence of the Cross Section in PWIA

The main quantity in which we are interested is the α-dependence of the $A(p, 2p)X$ quasielastic cross section at fixed-large c.m. angles and high momentum transfer. The reason of this choice is twofold: first, the α-dependence naturally expresses the sensitivity of the $A(p, 2p)X$ cross section to the high momentum component of the nuclear wave function which will be discussed below; second, as it will be demonstrated in the Section II F 2 the α variable is not sensitive to the soft initial and final state reinteractions of energetic protons with target nucleons. Thus its distribution will largely reflect the distribution of the nucleon within the SRC without substantial modification due to initial and final state interactions.

In Figure 2 we present the α-dependence of the $^{12}C(p, 2p)X$ cross section calculated for different values of incoming proton momenta. The calculations are within the PWIA framework described above. Here the c.m. angle of the $pp \to pp$ scattering is restricted

to 90 ± 5^0. The calculation is done for ^{12}C target using Harmonic Oscillator momentum distribution $n(k)$ in Eq.(5) and high momentum tail of the deuteron wave function calculated, using the NN Paris potential in Eq.(7), with $a_2(^{12}C) = 5$.

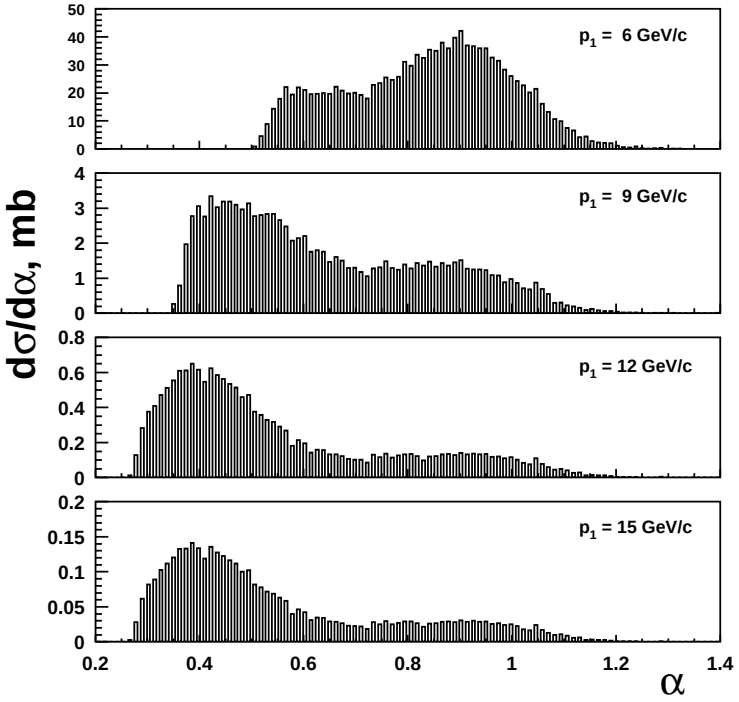

FIG. 2. PWIA calculation of the α-dependence of the $^{12}C(p, 2p)X$ cross section at different values of incident proton momenta.

Elastic pp scattering off a proton at rest corresponds to $\alpha = 1$. As can be seen from Figure 2, most of the strength is at $\alpha < 1$ which corresponds to a scattering off a proton with momenta in the direction of $\vec{p}_1$. This is a quantitative illustration of the discussion in the introduction: the *pp* cross section on bound proton scales with the total pp c.m. energy as $\sim (s\alpha)^{-10}$, therefore the $A(p, 2p)X$ cross section is dominated by smaller α.

One can clearly observe a double peak structure of the α-distributions. The first peak, closer to $\alpha = 1$, is due to scattering off a proton in the Fermi sea Eq.(5). The other peak, at even lower α values, is due to the scattering off the SRC Eq.(6). As the incoming energy increases, one can see the shift of the strength to the lower α-range which means more and more scattering off target protons with high Fermi momenta aligned in the direction of the incoming proton momentum p_1. This shift shows the onset of the regime where one expects to probe short-range nucleon correlations in the nucleus. This picture demonstrates the selectivity of hard $A(p, 2p)X$ reactions to the large values of the bound nucleon momenta in the nucleus, predicted originally in Ref. [10,11].

F. Competing Nuclear Effects

The calculations above were done within PWIA, using *pp* parameterization (Eq.(10)) for the scattering off a free proton. Two basic nuclear effects that can obscure the expected α-dependence are the modification of the bound protons in the nuclei and the initial and final state interactions of incoming and scattered protons respectively.

1. Nuclear Medium Modification of Bound Protons

We consider possible binding modifications of the bound nucleon structure which are consistent with the in medium deep-inelastic (DIS) nucleon structure functions measured using lepton-nucleus scattering - phenomenon known as the "EMC effect" [20]. One of the mechanisms that can account for the observed modification of DIS structure function is the suppression of point-like configurations (PLC) in a bound nucleon as compared to a free nucleon [21,10,22].

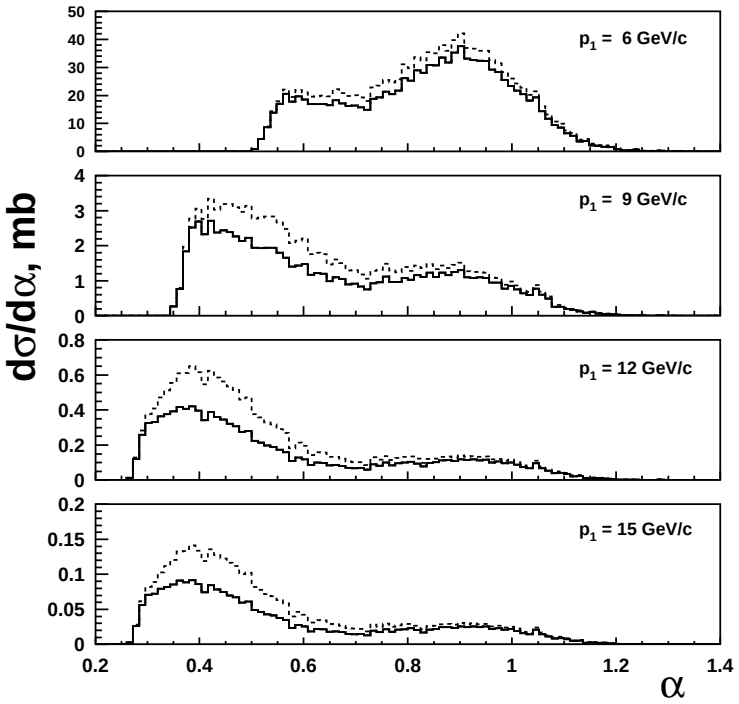

FIG. 3. The α-dependence of the cross section for different values of incident proton momenta. Dashed line - PWIA, solid line- with EMC effects discussed in the text. The kinematics are the same as for Fig. 2.

The PLC are small sized partonic configurations in the nucleons which due to the color screening are weakly interacting objects. In the color screening model of EMC [21,10], the binding of the nucleonic system results a suppression of the nucleon's PLC component. This suppression does not lead to a noticeable change in the average characteristics of a nucleon

in the nucleus. However, it is sufficient to account for the observed EMC effect in DIS scattering from nuclei. Since the high momentum transfer pp elastic scattering is mainly due to the scattering off a PLC in the protons, the expected suppression of PLC will reduce the cross section of pp scattering off bound proton. This suppression can be estimated by multiplying the free pp cross section of Eq.(10) by the factor [21]

$$\delta(k,t) = \left(1 + \Theta(t_0 - t) \cdot (1 - \frac{t_0}{t}) \cdot \frac{\frac{k^2}{m_p} + 2\epsilon_A}{\Delta E}\right)^{-2}, \tag{11}$$

where $\epsilon_A \approx 8\ MeV$ is the average nuclear binding energy and $\Delta E \approx 0.6 - 1\ GeV$ is a parameter that characterize a typical excitation of the bound nucleon. The t-dependence in Eq.(11) is due to the fact that in the wave function of a nucleon the PLC dominate at sufficiently high values of the momentum transfer [23] ($-t_0 \approx 2GeV^2$). As follows from Eq.(11) the $\delta(k,t)$ correction tends to reduce the expected α-shift shown in Figure 1, since it introduces additional α^l ($l \sim 2-3$) dependence, which softens the $(s\alpha)^{-10}$ dependence of the pp cross section in Eq.(2). Note that a similar suppression is expected within the rescaling model of the EMC effect [24,25]). On the other hand in a number of models of the EMC effect, such as pion and binding models (for review see [10]) the shift to $\alpha < 1$ is amplified as compared to the multinucleon calculation [11,34]. Thus, our estimation within the color screening model can be considered as the upper limit of possible suppression due to binding nucleon modification.

Using Eqs.(2,9,10,11) the calculated cross section is shown in Figure 3 as a function of α. As Figure 3 shows, the considered medium modification effect suppresses the high momentum strength of the cross section, since it corresponds to the larger virtualities of the bound nucleon, which are more sensitive to the PLC structure of nucleon. However, the suppression does not diminish the expected downward shift of the α-distribution. It would require very unreasonable modifications of the bound nucleon structure (contradicting the EMC effects in DIS) to make the α-shift (to the $\alpha < 1$ region) completely vanish.

2. The Effect of the Initial and Final State Interactions

The major nuclear effect which can obscure the information on SRC are the initial and final state interactions (ISI, FSI) of the incident and outgoing protons in the nuclear medium. Since the momenta of incoming and two outgoing protons are above a few GeV/c one can calculate these rescatterings in eikonal approximation.

For bound nucleons with small momenta $0.8 < \alpha < 1.2$ and $p_t \leq p_{Ferm}$, where the scattered and the knocked-out protons reinteract with uncorrelated nucleons, we apply the conventional Glauber approximation to calculate the small angle rescatterings. This is justified since in these cases the spectator nucleons can be considered as a stationary scatterers. Integrating over a wide range of the missing energy of the $A(p,2p)X$ reaction allows to simplify further the calculation of ISI/FSI using the probabilistic approximation of Ref. [27], which accounts for all orders (single, double, etc) of the soft pN rescatterings.

However, the above approximation cannot be used for the bound protons in SRC (which have a large value of Fermi momentum). There, the spectator nucleon cannot be treated

as a stationary scatterer and therefore the Glauber approximation is not valid (see e.g. [28]). To calculate the initial and final state rescatterings in this case we assume that for incoming and outgoing protons the first rescattering most probably happens with the partner nucleon in the SRC. Indeed, as it was demonstrated in Ref. [15], because of the large virtuality of interacting nucleon in SRC the distance of the first soft reinteraction after the point of hard interaction is less than 1 fm and it decreases with the increase of t and p_2. Within the framework of two-nucleon correlation model one can account for the soft rescatterings in the SRC using the calculation of $d(p,2p)n$ reaction in Generalized Eikonal Approximation (GEA), Ref. [28,29]. Using the GEA we only calculate the single rescatterings of the incoming and knocked-out protons with the correlated nucleon (Figure 4 b,c,d). The main feature of the GEA is that it accounts for the nonzero values of spectator nucleon momentum (it does not treat the spectator as a stationary scatterer as being done in the conventional eikonal approximation). This feature is especially important in the SRC region since in this case the correlated nucleon momenta are large and can not be neglected.

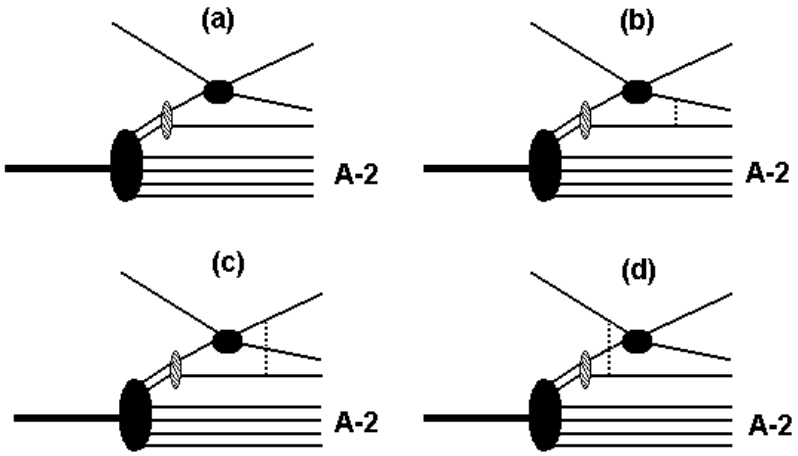

FIG. 4. Diagrams describing PWIA (a), final (b,c), and initial (d) state reinteractions for two-nucleon correlations

The effect of the rescatterings in the SRC (in the range of $\alpha < 0.8$ or $\alpha > 1.2$) can be accounted for by introducing a correction factor κ which multiplies the SRC spectral function of Eq.(9). We define κ as follows:

$$\kappa = \frac{|F_a + F_b + F_c + F_d|^2}{|F_a|^2}, \tag{12}$$

where F_a is the PWIA amplitude, and F_b, F_c and F_d are the single rescattering amplitudes corresponding to $p + (NN)_{SRC} \to p + N + N$ scattering shown in Figure 4. To obtain the F's we use the rescattering amplitudes for the $d(p,pp)n$ reaction calculated in Ref. [29]:

$$F_{(j)} = -\frac{(2\pi)^{\frac{3}{2}}}{4i} A_{pp}^{hard}(s,t) \int \frac{d^2k_t}{(2\pi)^2} f^{pN}(k_t)(\psi_d^{\mu}(\tilde{p}_s^{(j)}) - n \cdot i\psi'^{\mu}(\tilde{p}_s^{(j)})), \tag{13}$$

where j(n)=b(1),c(1),d(-1). A_{pp}^{hard} is the amplitude of the pp hard scattering which, within the factorization approximation, cancels in κ. f^{pN} is the amplitude of a small angle (soft)

pN scattering, N can be either proton or neutron. ψ_d is the deuteron wave function and ψ' accounts for the distortion due to FSI (see Ref. [29]).

For higher order rescatterings we applied the probabilistic approximation of Ref. [27] which we used already in the case of small Fermi momenta. This is justified since in the kinematics of two-nucleon SRC the second and higher order rescatterings happen outside of the SRC. It is worth noting that the error originating from the last approximation is rather small since for the intermediate size nuclei ($A \sim 12-16$) the overall contribution of higher order rescatterings in the considered kinematics of the $A(p,2p)X$ reaction is small (a few percent as compared with the single rescattering contribution [27]).

It is important to emphasize that the major qualitative feature of reinteractions with uncorrelated nucleons, in high energies, is the existence of the approximate conservation law for the light cone momenta of interacting particles [28,30]. Namely, for energetic particles small angle soft reinteractions do not change the α- distribution.

To demonstrate this let us consider the propagation of fast nucleon with momentum $p_1 = (E_1, p_1^z, 0)$ through the nuclear medium. After the small angle reinteraction of this nucleon with a nucleon in the nucleus with momentum $p_2 = (E_2, p_2^z, p_2^t)$, the energetic nucleon still maintains its high momentum and leading z-direction having now a momentum $p_1' = (E_1', p_1^{z\prime}, p_1^{t\prime})$ with $\frac{<(p_1^{t\prime})^2>}{(p^{z\prime})^2} \ll 1$. The other nucleon momentum after the collision is $p_2' = (E_2', p_2^{z\prime}, p_2^{t\prime})$. The energy momentum conservation for this scattering allows us to write for the "α" component:

$$\alpha_1 + \alpha_2 = \alpha_1' + \alpha_2' \equiv \frac{p_{1-}}{m} + \frac{p_{2-}}{m} = \frac{p_{1-}'}{m} + \frac{p_{2-}'}{m}. \tag{14}$$

The change of the α_2 ("$-$") component due to rescattering can be obtained from Eq.(14):

$$\Delta\alpha_2 \equiv \frac{\Delta p_{2-}}{m} = \frac{p_{2-} - p_{2-}'}{m} = \frac{p_{1-}' - p_{1-}}{m} \ll 1. \tag{15}$$

which means:

$$\alpha_2' \approx \alpha_2. \tag{16}$$

In Eq.(15) we use the conditions $\frac{p_{1-}'}{m}, \frac{p_{1-}}{m} \ll 1$ which is well satisfied in the small angle reinteractions since $\frac{<(p_1^{t\prime})^2>}{(p^{z\prime})^2} \ll 1$. Thus, with the increase of the incident energy a new approximate conservation law is emerging: α_2 is conserved by ISI/FSI. The uniqueness of the high energy rescattering is in the fact that although both the energy and the momentum of the nucleons are distorted by the rescattering, the combination of $E_2 - p_2^z$ is almost not affected. In the same way the rescattering of the incoming and two outgoing protons in the (p,2p) reaction conserve the reconstructed α-component of the target proton. Therefore the α-distribution measured in $A(p,2p)X$ reaction reflects well the original α-distribution of the target proton in the nucleus. A numerical estimate of this conservation will be presented in the next section.

To complete the discussion on ISI/FSI we should mention that for incident proton momenta exceeding $6-9$ GeV/c the Glauber approximation overestimates the absorption of protons if compared with the data of Ref. [31,32]. The overestimate of the absorption in

these experiments is attributed to the Color Transparency (CT) phenomena, in which it is assumed that the hard $pp \to pp$ primary process in the $A(p,2p)X$ reaction is dominated by the interaction of protons in the point like qqq configurations. As a result, immediately before and after the hard interaction the color neutral PLC has a diminished strength for ISI/FSI reinteraction. Since the PLC is not an eigenstate of QCD Hamiltonian (free nucleons have a finite size) the interaction strength will evolve to the normal hadronic interaction strength in parallel with the evolution of PLC to the normal hadronic size during the propagation of the fast proton in the nuclear medium. We estimate the CT phenomenon within the quantum diffusion model of Ref. [33]. This model which describes reasonably well [23] the data [31] assumes the following amplitude for the $PLC-N$ soft interaction:

$$f^{PLC,N}(z,k_t,Q^2) = i\sigma_{tot}(z,Q^2)\cdot e^{\frac{b}{2}t}\cdot \frac{G_N(t\cdot\sigma_{tot}(z,Q^2)/\sigma_{tot})}{G_N(t)}, \tag{17}$$

where $b/2$ is the slope of elastic NN amplitude, $G_N(t)$ ($\approx (1-t/0.71)^2$) is the Sachs form factor and $t=-k_t^2$. The last factor in Eq.(17) accounts for the difference between elastic scattering of PLC and average configurations, using the observation that the t-dependence of $d\sigma^{h+N\to h+N}/dt$ is roughly that of $\sim\ G_h^2(t)\cdot G_N^2(t)$ and that $G_h^2(t)\approx exp(R_h^2 t/3)$, where R_h is the rms radius of the hadron.

In Eq. (17) $\sigma_{tot}(l,Q^2)$ is the effective total cross section for the PLC to interact at distance l from the hard interaction point and σ_{tot} is the pN total cross section. The quantum diffusion model [33] predicts:

$$\sigma_{tot}(,Q^2) = \sigma_{tot}\left\{\left(\frac{z}{l_h}+\frac{\langle r_t(Q^2)^2\rangle}{\langle r_t^2\rangle}(1-\frac{z}{l_h})\right)\Theta(l_h-z)+\Theta(z-l_h)\right\}, \tag{18}$$

where $l_h = 2p_f/\Delta\ M^2$, with $\Delta\ M^2 = 0.7-1.1\ GeV^2$. Here $\langle r_t(Q^2)^2\rangle$ is the average squared transverse size of the configuration produced at the interaction point. In several realistic models considered in Ref. [34] it can be approximated as $\frac{\langle r_t(Q^2)^2\rangle}{\langle r_t^2\rangle}\sim\frac{1\,GeV^2}{Q^2}$ for $Q^2\ \geq\ 1.5\ GeV^2$. Note that due to expansion, the results of the calculations are rather insensitive to the value of this ratio whenever it is much less than unity. For numerical calculations we assumed $\Delta M^2\approx 0.7 GeV^2$ as was chosen to describe the nuclear transparencies from $A(p,2p)X$ [31] and $A(e,e'p)X$ [35] experiments (see comparisons in Ref. [23]).

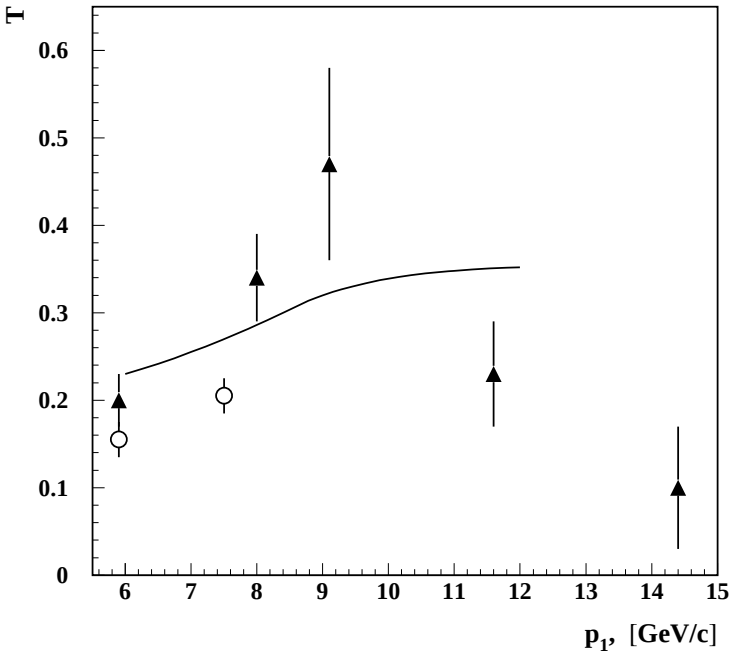

FIG. 5. The p_1-dependence of the transparency T calculated within quantum diffusion model. Data marked by triangles and circles are from [32] and [36] respectively.

In Figure 5 we compares the prediction of quantum diffusion model for nuclear transparency T with the data of the EVA experiment [12,32]. The transparency T is defined as the ratio of the $A(p,2p)X$ cross section calculated using PWIA, color screening and rescattering effects to the cross section calculated within PWIA only. The comparison shows that one has a fair agreement with the data up to 9 GeV/c incoming proton momenta (note that one expects that the probabilistic model of rescattering to work within 20% accuracy). The decrease of the experimental values of transparency can be understood in terms of the interplay of the hard and soft component in the amplitude of high momentum transfer pp scattering [37,17] which is not incorporated in the current calculations. Since in the further analysis we will concentrate only in the region of incoming proton momenta $5.9 \leq p_1 \leq 7.5 GeV/c$ where this interplay does not play a role, we will use the simple formulae of Eqs.(17,18) for numerical estimations. The detailed analysis of the energy dependence of the nuclear transparency, T will be presented elsewhere.

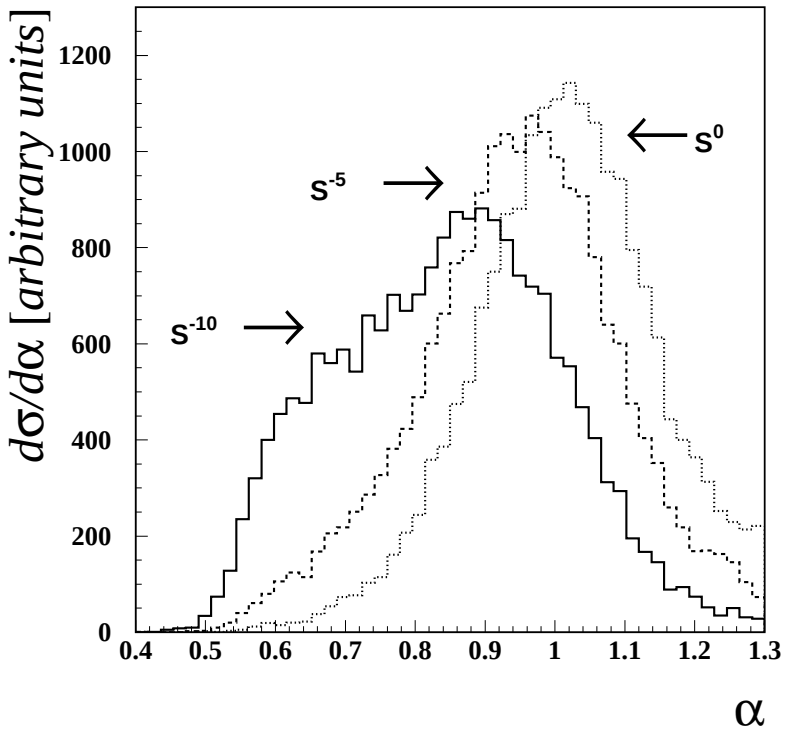

FIG. 6. The α-dependence of the $A(p,2p)X$ cross section for different assumed s-dependences of the hard elastic pp scattering cross section.

III. RESULTS OF THE MODEL

In the following chapter we discuss the results of the model presented in Chapter II, for several nuclear observables that can be measured in the $A(p,2p)X$ reaction. We are particularly interested in two kinds of information: how the substructure of high-momentum transfer pp scattering reveals itself in the nuclear reaction and what kind of information one can infer about short-range nuclear structure from these reactions. For numerical calculations in this chapter we apply the kinematics of EVA experiment [12]. Because of the multidimensional character of the kinematical restrictions the numerical calculations are implemented through the Monte Carlo calculation. Furthermore, we will present the cross sections in arbitrary units since we are interested mainly in the shapes of the α and p_t dependence of the $A(p,2p)X$ cross section.

A. How the Quark Substructure of Hard pp Scattering is being Reflected in the Nuclear Observables

The power law energy-dependence of the hard elastic pp scattering cross section is the signature of the dominance of quark-gluon degrees of freedom in the high-momentum transfer scattering (see e.g. [1]). As was predicted in Ref. [11] if this strong energy-dependence ($\sim s^{-10}$) exists in the nuclear medium it will amplify the contribution to the cross section

coming from the scattering off deeply bound protons. These protons have a large momentum in the direction of the incoming proton.

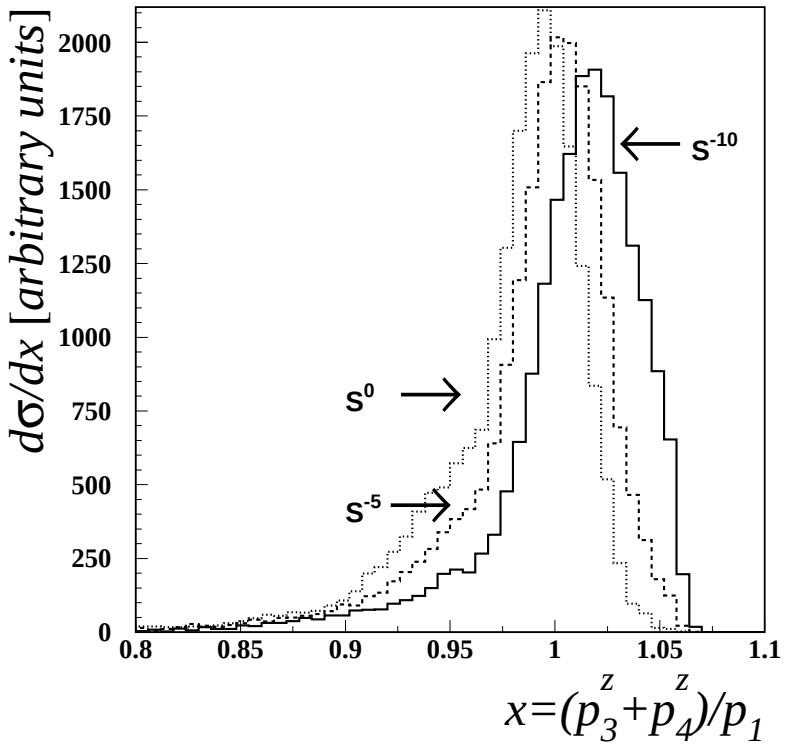

FIG. 7. The x-dependence of the cross section for different hard elastic pp scattering power laws.

Since the cross section for the high-momentum transfer scattering of incoming proton off the bound proton at fixed and large $\theta_{cm} \sim 90^0$ is roughly proportional to $(\alpha s)^{-10}$ (see Eqs.(2-10)), an observation that reflects the sensitivity of $A(p,2p)X$ reaction to the high momentum component of the nuclear wave function is the shift of the α-spectra to the lower α values. To demonstrate this sensitivity, in Figure 6 we represent the α-dependence of the $A(p,2p)X$ reaction cross section assuming different s-dependences of the cross section for hard $p+p \to p+p$ scattering. These calculations are merely for illustration of the connection between the s-dependence and the α-shift. Figure 6 confirms that the larger is the negative power of s-dependence for the hard pp scattering the larger is the average longitudinal momentum of the interacting bound nucleon ($\alpha < 1$).

The α-shift also produces an excess of the total longitudinal momentum of the final outgoing protons as compared to the initial longitudinal momentum p_1. One can characterize this excess through the variable:

$$x = \frac{p_3^z + p_4^z}{p_1}, \tag{19}$$

which will increase as the power of the hard pp scattering cross section increases. In Figure 7 we show the calculated x-dependence of the cross section for different assumed s-dependences. The expected shift to the higher x (lower α) is clearly seen in Figure 7. The

x-distribution for quasielastic $C(p,2p)X$ reactions peaks at $x < 1$, if one assumes no s-dependence of the elementary $p + p \to p + p$ reaction. As the dependence on s increases the peak is shifted to $x > 1$ which represents the nuclear "boosting" effect: the outgoing protons have more longitudinal momentum than the incoming momentum. It is worth noting that this effect is reminiscent of subthreshold production in nuclei, in which a very low available energy in the nuclear medium can cause dramatic changes in the cross section of the reaction.

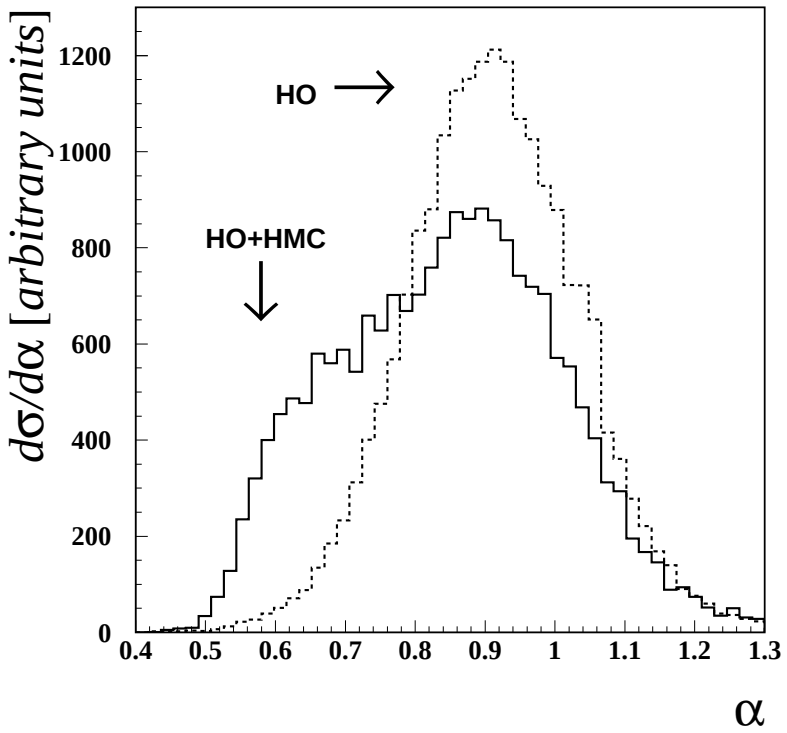

FIG. 8. The $\alpha-$dependence of the cross section calculated for two models of the nuclear wave functions. "HO" is Harmonic Oscillator and "HO+HMC" - corresponds to the short range correlation model of Section II C. The $A(p,2p)X$ cross section is calculated within PWIA at $p_1 = 6\ GeV/c$ and $\theta_{cm} = 90^0$.

B. Sensitivity to Short Range Correlations in Nuclei

The next question we would like to address is the sensitivity of the α-shift to the existence of high momentum components in the nuclear ground state wave function. To asses this sensitivity we compare the cross sections of the $A(p,2p)X$ reaction using two models for the nuclear wave function: an Harmonic Oscillator (HO) model and the two-nucleon SRC model of high momentum component (HMC) of nuclear wave function, described in Section II C (HO+HMC). In Figure 8 we present the α-dependence of the $A(p,2p)X$ cross section calculated within PWIA at $p_1 = 6\ GeV/c$ and $\theta_{cm} = 90^0$ using these two models.

As Figure 8 shows, even at moderate energies as $p_1 = 6\ GeV/c$ the α- dependence shows substantial sensitivity to the high momentum structure of the nuclear wave function. Thus,

the measured cross section at small α will allow us to obtain the characteristics of the high momentum tail of the wave function.

In Figure 9, we show the results of the PWIA calculations for transverse momentum distribution of the cross section of $A(p,2p)X$ reaction. It also exhibits a sensitivity to the high momentum part of the nuclear wave function. However, as will be shown below, unlike the α-distribution the transverse momentum distribution is strongly distorted due to the initial and final state interactions. Note that hereafter, for the transverse missing momentum distribution, we will consider only the p_y component of p_t. This restriction is related to the fact that the experimental data have better resolution for the p_y component of missing momentum.

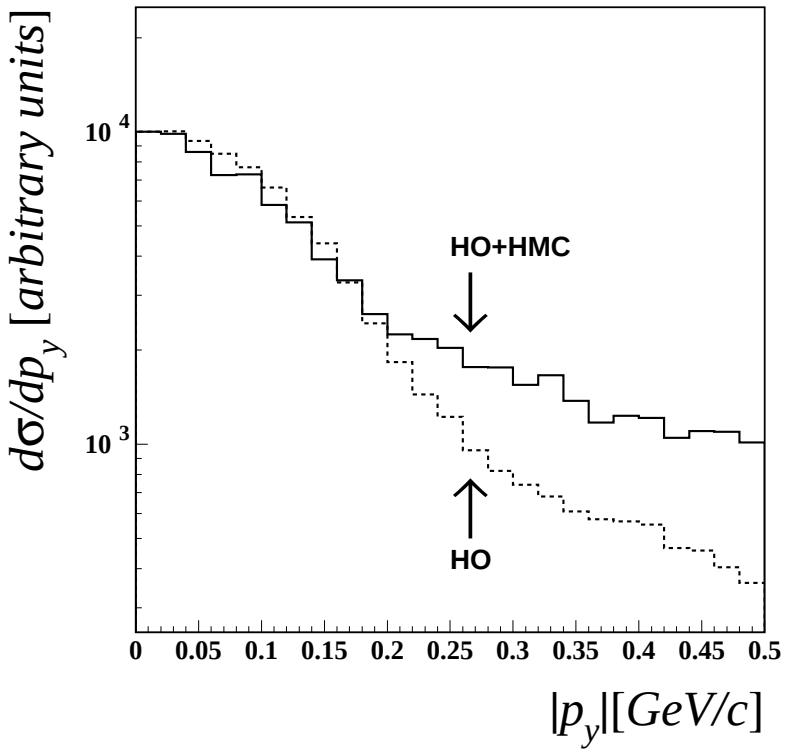

FIG. 9. The p_y-dependence of the cross section for the two models of nuclear wave functions described in the text. The kinematics of the calculations and notations are the same as in Fig. 8.

C. The Effect of Initial and Final State interactions

As was discussed in Chapter 2 (see Eq.(15)) one expects that the soft rescatterings with uncorrelated nucleons at high energies will conserve the α parameter of interacting nucleons. Thus the measured α_2-distribution of $A(p,2p)X$ cross section will not be affected strongly by the ISI/FSI and will reflect the original α-distribution of the target proton in the nucleus.

In Figure 10 we compare the p_2 and α distribution of the $\theta_{cm} = 90^0$ $A(p,2p)X$ differential cross section at $p_1 = 6$ GeV/c. The dashed lines correspond to the PWIA prediction, thus representing the "true" momentum distribution of the bound nucleon. The solid lines represent the calculation including ISI/FSI. In the latter case the p_2 and α are reconstructed

through the momenta of the incoming (p_1) and outgoing protons (p_3, p_4), thus representing the "measured" quantities.

Notice the effect of the ISI/FSI on the p_2-distribution versus the effect of the same ISI/FSI on the α-distribution. As we mentioned before, both the reconstructed energy and momentum of the target proton are modified by the rescattering, but their linear combination, α, is almost unchanged.

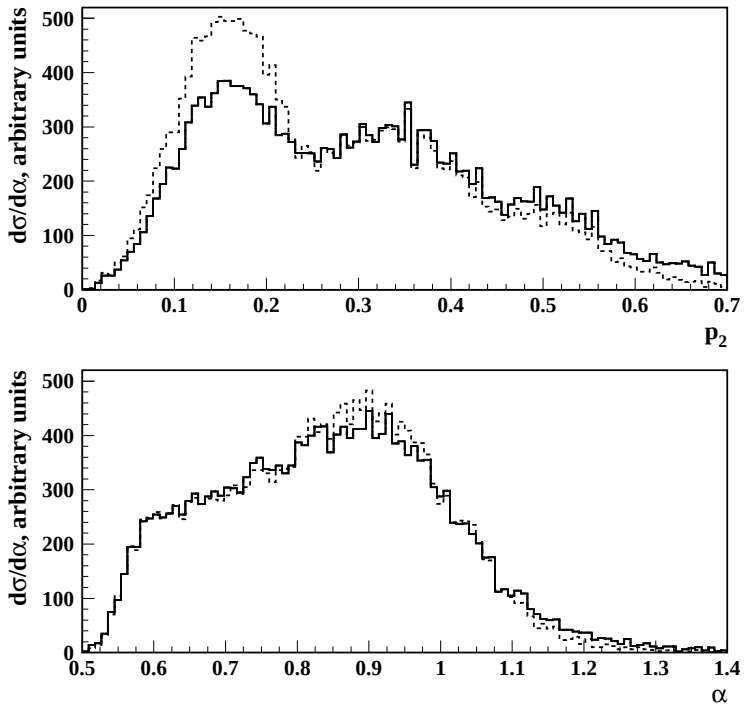

FIG. 10. The α-dependence of the cross section with and without rescattering with uncorrelated nucleons.

Finally, in Figure 11 we show the transverse momentum distribution (p_y) calculated for the same kinematics as in Figure 10. Figure 11 shows substantial ISI/FSI effects on the p_y-distribution for both calculation with and without Color Transparency. The large contribution from ISI/FSI in the transverse momentum distribution is attributed to the structure of small angle hadronic interaction in high energies. The rescattering is mainly transverse thus affecting maximally the transverse momenta of interacting nucleons.

The above discussion allows us to conclude that the experimental study of the α-distribution provides direct information on high momentum components of the nuclear wave function. On the other hand, the large values of missing transverse momentum is mainly sensitive to the dynamics of initial and final state interaction. In the subsequent sections we will discuss the analysis of the first experimental data on $A(p, 2p)X$ reaction.

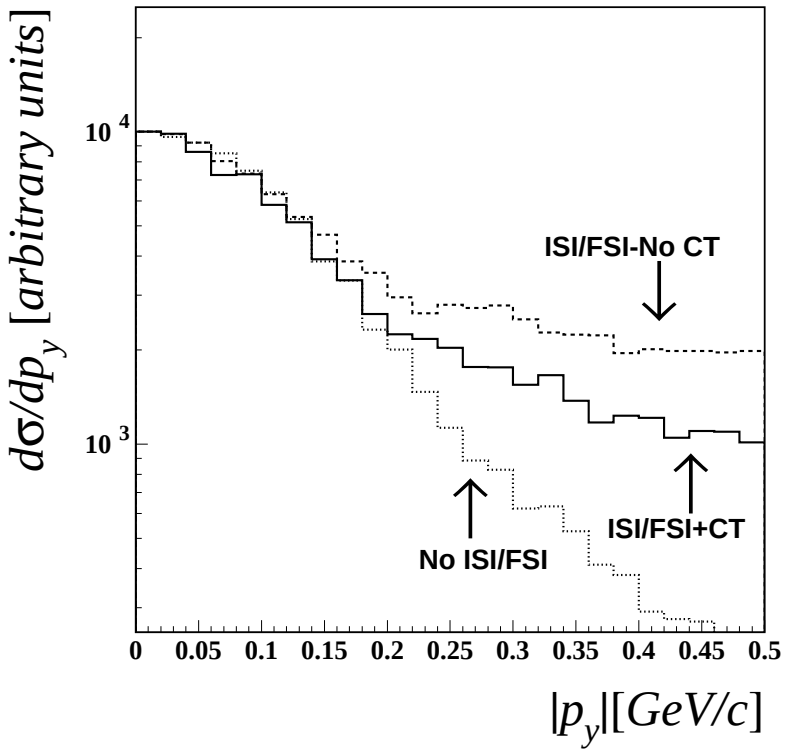

FIG. 11. The p_y dependence of the cross section with and without rescattering effects.

IV. MEASUREMENTS AND DATA.

We compare the calculations with the data that were collected in EXP 850 using the EVA spectrometer at the AGS accelerator of Brookhaven National Laboratory. During the preparation of this work these data were the only ones on high momentum transfer quasi-elastic reactions [12]. In this chapter we will briefly describe the experiment and the experimental procedures relevant for comparing the data with the calculations. In the following chapter we will present the calculations and compare them with the data.

The EVA collaboration performed a second measurement over a wider kinematical range with incident momenta above 7.5 GeV/c. These data were not analyzed yet. Some of the calculations in this work are predictions for these new data which might become later available.

A. The Experimental Setup

The EVA spectrometer, located on the secondary line C1, consisted of a 2 meter diameter and 3 meter long super-conducting solenoidal magnet operated at 0.8 Tesla (see Fig 12). The beam entered along the z axis and hit a series of targets located at various z positions. The scattered particles were tracked by four cylindrical chambers (C1-C4 , Fig 12). Each had 4 layers of long straw drift tubes with a high resistance central wire. For any of the 5632 tubes that fired, the drift time to its central wire was read out. In three out of the four

cylindrical chambers signals were read out at both ends, providing position information along the z direction as well. The straw tubes information allowed the target identification, the measurement of the particles transverse momentum as they were bent in the axial magnetic field, and their scattering angles. The overall resolution caused by the beam, the target and the detector were determined from the two body elastic pp scattering measurement. The standard deviation (σ) for the resolution of the transverse momentum is $\Delta p_t/p_t = 7\%$ and 0.27 GeV for the missing energy. The polar angles (θ_3,θ_4) of the two outgoing protons were measured with a resolution of 7 mrad. The beams ranged in intensity from 1 to $2 \cdot 10^7$ over a one second spill every 3 seconds. Two counter hodoscopes in the beam (only one shown in fig 12) provided beam alignment and a timing reference and two differential Cerenkov counters (not shown in fig 12) identified the incident particles. Three levels of triggering were used to select events with a predetermined minimum transverse momentum. The first two hardware triggers selected events with transverse momenta $p_t > 0.8$ and $p_t > 0.9$ GeV/c, for the 6 and 7.5 GeV/c measurements, respectively. The third level software trigger required two almost coplanar tracks, each satisfying the second level trigger requirement and low multiplicity hits in the straw tubes. See Ref [39] for a detailed description of the trigger system. Details on the EVA spectrometer are given in Refs. [39–42].

Three solid targets, CH_2, C and CD_2 (enriched to 95%) were placed on the z axis inside the C1 cylinder separated by about 20 cm. They were 5.1x5.1 cm^2 squares and 6.6 cm long in the z direction except for the CD_2 target which was 4.9 cm long. Their positions were interchanged at several intervals in order to reduce systematic uncertainties and to maximize the acceptance range for each target. Only the C target was used to extract the QE events, while the other targets served for normalizations and references.

B. Event Selection and Kinematical Constraints

Quasi-elastic scattering events, with only two charged particles in the spectrometer, were selected. An excitation energy of the residual nucleus $\mid E_{miss} \mid < 500$ MeV was imposed in order to suppress events where additional particles could be produced without being detected in EVA. Since this cut is above m_π, some inelastic background, such as those coming from $pA \rightarrow pp\pi^0(A-1)$ events, could penetrate the cuts and had to be subtracted. The shape of this background was determined from a fit to the E_{miss} distribution of events with extra tracks in the spectrometer. An inelastic background with this shape was subtracted. The measured distributions represent background subtracted quantities. See Refs. [42,12] for more details.

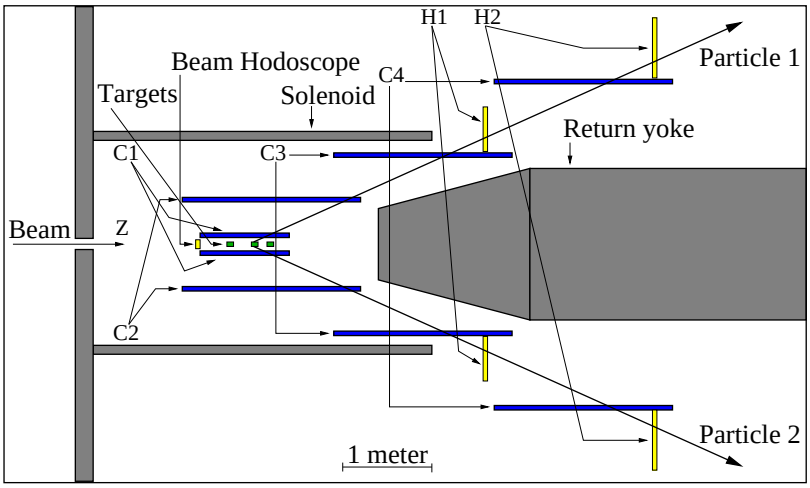

FIG. 12. A schematic view of the EVA spectrometer. C1-C4 are the straw tube 4 layers detectors. H1-H2 are scintillator hodoscopes used for fast triggering on high p_t events. The three targets in C1 are shown in typical positions. The beam direction (symmetry axis of the detector) is chosen to be the z axis. Not shown in the figure are the beam counters upstream the spectrometer as well as the full iron structure around the solenoid.

The coordinate system was chosen with the z coordinate in the beam direction and the y direction normal to the scattering plane (x, z). The latter is defined by the incident beam and one of the emerging protons. The selection among the two was random. This arbitrariness in the selection does not affect the extracted quantities of interest. The data were analyzed in terms of the momenta in the y direction p_y and the light cone α variable.

α was determined with a precision of $\sigma \simeq 3\%$. The p_y (perpendicular to the scattering plane) had a resolution of $\sigma = 40$ MeV/c. The resolution in p_x (in the scattering plane) was $\sigma = 170$ MeV/c. Because of its better resolution, p_y was used to represent a transverse component.

The laboratory polar angles of both detected protons were limited by a software cut to a region of $\pm(3-5)^o$ around the center of the angular acceptance, for each target position. The angular range enforced by the software cut is smaller than the geometrical limits of the spectrometer (see Fig 12) but it ensures a uniform acceptance. Since the experiment was focused on shapes and not absolute values, an acceptance correction in the (θ_3, θ_4) plane is not needed. An explicit cut on the center of mass scattering angle θ_{cm} was not applied on the data, however the cuts on the laboratory polar angles limit the θ_{cm} to the range of 83^o to 90^o for the proton at rest kinematics.

C. The Longitudinal (α) Distributions

Each target position corresponds to a limited polar angular range (θ_3, θ_4) and α is a strong function of $\theta_3 + \theta_4$. To cover the largest possible acceptance in α one has to merge the measured α-distributions from different targets. The distributions from the individual target positions were normalized to each other using the overlapping regions. The experimental

error in each bin includes also the relative normalization error. The value of $\mid \theta_3 - \theta_4 \mid$ was limited by the largest common acceptance of all target position.

To summarize: the following angular acceptance cuts were applied on the data:

- $\mid \theta_3 - \theta_4 \mid < 0.06$ radians (For all target positions and both beam energies).
- downstream target: $23.5^0 < \theta_3 < 32.0^0$ and $23.5^0 < \theta_4 < 29.5^0$ or θ_3 and θ_4 inverted.
- middle target: $20.0^0 < \theta_3 < 30.0^0$ and $22.0^0 < \theta_4 < 28.0^0$ or θ_3 and θ_4 inverted.
- upstream target: $19.0^0 < \theta_3 < 28.0^0$ and $21.0^0 < \theta_4 < 27.5^0$ or θ_3 and θ_4 inverted.

These cuts yield for 5.9 GeV/c the following α acceptance ranges:

- downstream target: $0.9 < \alpha < 1.05$.
- middle target: $0.767 < \alpha < 0.967$.
- upstream target: $0.7 < \alpha < 0.867$.

For the 7.5 GeV/c data the angular ranges were:

- downstream target: $22.0^0 < \theta_3 < 32.0^0$ and $22.0^0 < \theta_4 < 31.5^0$ or θ_3 and θ_4 replaced.
- middle target: $21.0^0 < \theta_3 < 27.0^0$ and $21.0^0 < \theta_4 < 27.0^0$.
- upstream target: $20.0^0 < \theta_3 < 26.0^0$ and $20.0^0 < \theta_4 < 26.0^0$.

These cuts yield for 7.5 GeV/c the following α acceptance ranges:

- downstream target: $0.967 < \alpha < 1.05$.
- middle target: $0.834 < \alpha < 1.0$.
- upstream target: $0.767 < \alpha < 0.934$.

D. The Transverse (p_y) Distributions

The p_y-distributions were studied for narrow regions of α. The regions of α were chosen to yield a large overlap between the 5.9 GeV/c and the 7.5 GeV/c data sets for each target position:

- $0.74 < \alpha < 0.84$ for the upstream target position.
- $0.82 < \alpha < 0.92$ for the middle target position.
- $0.95 < \alpha < 1.05$. for the downstream target position.

The shape of the p_y- distributions for the two data at 6 and 7.5 GeV/c are consistent in each one of the three α- regions. Since the data sets of the two energies were found to be consistent they were added in order to reduce the statistical errors. Even after this procedure the poor statistics for the $0.95 < \alpha < 1.05$ range do not allow us to draw conclusions for this range. All the data presented consist of events that passed all the quasi-elastic cuts and the residual inelastic background was subtracted in a way similar to that described for the α- distributions (see Ref. [12,42] for details). All measured p_y- distributions are normalized to 10000 at $p_y = 0$ and shown on a logarithmic scale to emphasize their shapes. The data are compared to the calculations in chapter 5.

V. COMPARISON OF THE CALCULATIONS WITH THE DATA

A. The Longitudinal (α) Distributions

As was mentioned in Chapter 3 the calculations are implemented through the Monte Carlo code which allowed to incorporate the theoretical calculations with the multidimensional kinematic cuts applied in the experiment. The following cuts have been included in the calculations:

- The angular and α acceptances are constrained for the same ranges as presented in chapter IV for the data.
- $60^0 < \theta_{cm} < 120^0$ (for all target positions).

The calculations include all considered nuclear effects (EMC, ISI/FSI and CT).

Figure 13 shows the measured longitudinal α-distributions at 5.9 GeV/c and 7.5 GeV/c together with the calculations. In the calculation we used the two-nucleon correlation model for the high momentum component of the nuclear wave function, discussed in Chapter II. For the parameter $a_2(^{12}C)$ which defines the strength of the SRC in the nuclear spectral function (Eq.(9)) we used the estimate obtained from the analysis of high Q^2 and large Bjorken x $A(e,e')X$ data Ref. [15]. This analysis yield $a_2 \approx 5$ for ^{12}C.

The χ^2 per degree of freedom obtained by comparing the measured and calculated distributions at 5.9 GeV/c and 7.5 GeV/c ($\chi^2 = 0.8$ and $\chi^2 = 2.0$ respectively) confirm that the calculation and the data have the same shape.

The next question we ask is whether the data allow us to understand the ingredients contributing to the strength of the α-distribution at lower α-values.

First we check if the high momentum transfer elastic pp scattering off bound nucleon still attains the s^{-10} energy dependence. In Figure 14 we compare the calculations done using s-independent pp cross section (triangle points) and the pp cross section parameterized according to Eq.(10), in which $\frac{d\sigma^{pp}}{dt} \propto s^{-10}$ (solid points). If there was no scaling for hard pp scattering in the nuclei the α-distribution would peak around $\alpha = 1$, as shown by the calculations with no "s-weighting" (triangles). The data clearly show a shift to lower α which confirms the strong s-dependence of the quasi elastic process.

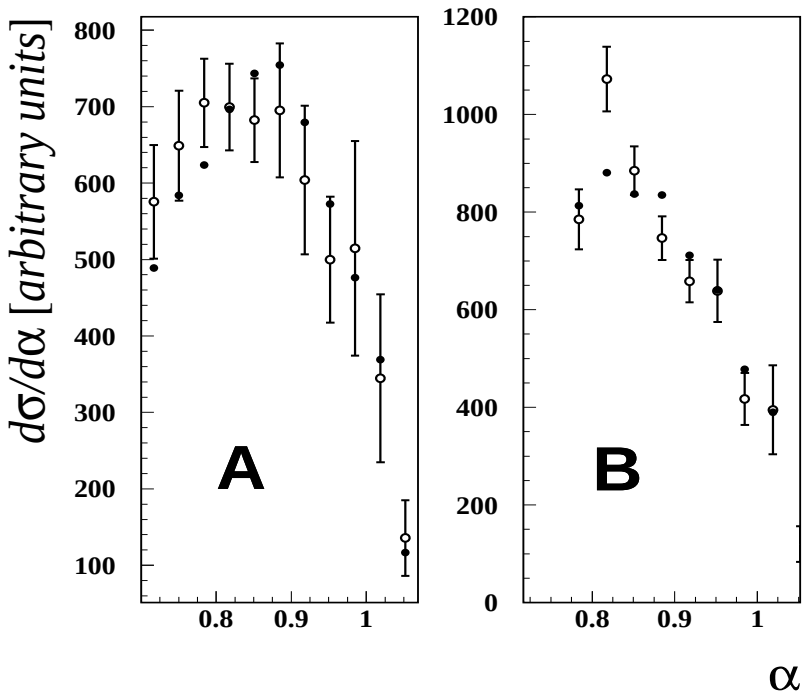

FIG. 13. A comparison between calculated α-distributions ($\bullet$) and the experimental data ($\circ$) at 5.9 GeV/c (A) and 7.5 GeV/c (B).

Next we address the question whether the strength seen at $\alpha < 1$ comes from the SRC in nucleus. Figure 15 shows two calculated α-distributions for the incoming proton momentum of 5.9 GeV/c. One distribution is calculated with the harmonic oscillator wave function only (i.e. $a_2 = 0$, in Eq.(9)) (Triangle points). The second distribution is calculated with the SRC contribution to the high momentum tail of the nuclear wave function, described by $a_2 = 5$ (solid points). The open circles are the data. It is clearly seen in the figure that the α-distribution calculated with $a_2 = 0$ does not provide sufficient strength at low α to describe the data, and SRC contributions are necessary.

It is important to note that both the strong s-dependence of hard pp scattering and the contribution of SRC are needed for agreement with the data. A mean field wave function for the nucleus would require a very unreasonable (exponentially falling with s) energy dependence of the pp scattering cross section, in order to explain the observed strength of the cross section at $\alpha < 1$. Moreover the agreement with the data using the same value of a_2 parameter obtained from electronuclear reactions indicates that we are dealing with a genuine property of the nucleus that does not depend on a specific probe.

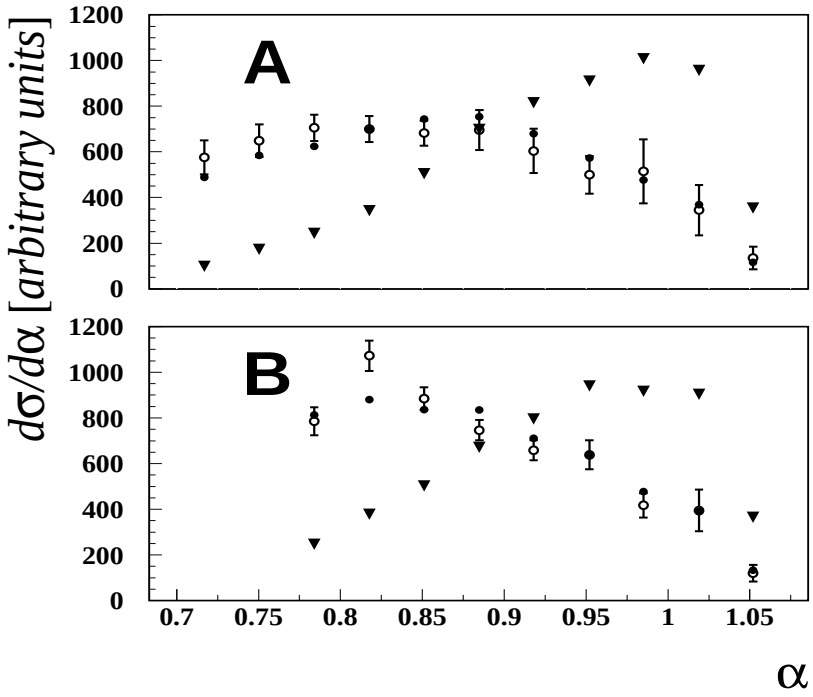

FIG. 14. Calculated longitudinal α-distributions with ($\bullet$) and without (∇) "s-weighting" compared to the measured data ($\circ$), at 5.9 GeV/c (A) and 7.5 GeV/c (B).

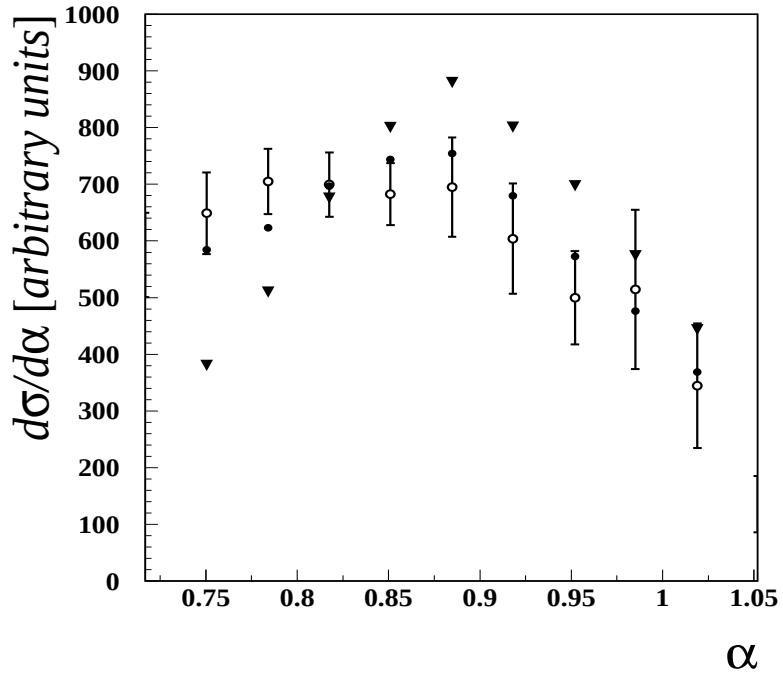

FIG. 15. Longitudinal α-distributions for 5.9 GeV/c.($\circ$ - data, ∇ - calculations with $a_2 = 0$, $\bullet$ - calculations with $a_2 = 5.0$).

B. The Transverse (p_y) Distributions

As it was discussed in Sections II and III, we expect the transverse missing momentum of the quasielastic $A(p,2p)X$ cross section to be sensitive mainly to the dynamics of ISI/FSI. The studies of electro-nuclear $A(e,e'p)X$ reactions, in which FSI occurs through the rescattering of only one knocked-out proton demonstrated that the eikonal approximation can describe the FSI with better than 10% accuracy (see e.g. [43]). This indicates that the expected level of accuracy in calculations of ISI/FSI in $A(p,2p)X$ reactions, in which one incoming and two outgoing protons undergo the soft rescatterings, will be on the order of 15-20%. Keeping these accuracies in mind we compare the theoretical calculations with the data checking how well the probabilistic approximation of ISI/FSI can reproduce the shape of the transverse missing momentum distribution.

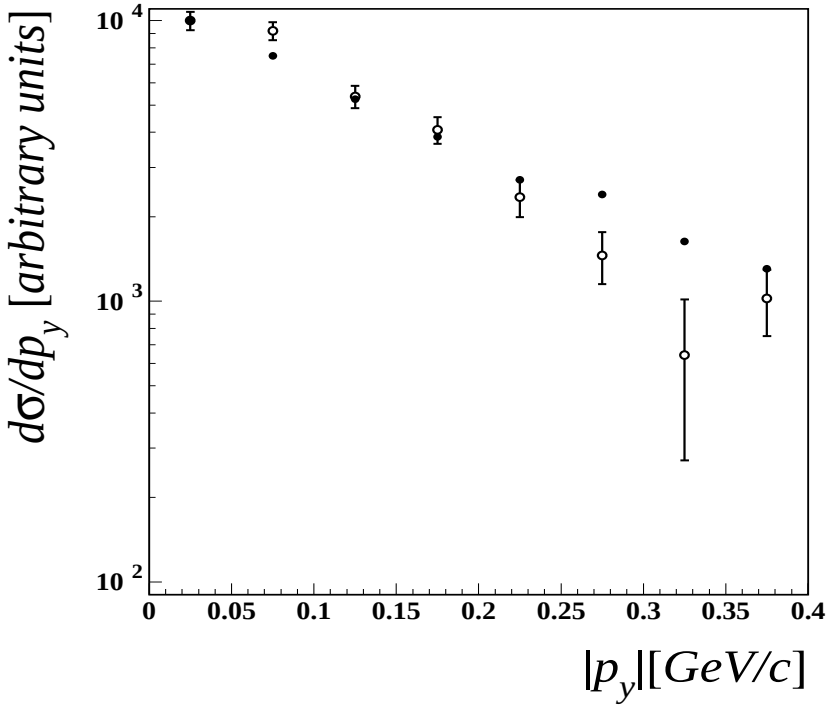

FIG. 16. A comparison between the calculated (•) and experimental (◦) p_y-distribution combined for 5.9 GeV/c and 7.5 GeV/c momenta. The kinematics for the upstream target with $0.74 < \alpha < 0.84$ is used (see text for details).

The following kinematical constraints are imposed in the Monte Carlo calculations

- middle target: $0.82 < \alpha < 0.92$.
- upstream target: $0.74 < \alpha < 0.84$.
- $\mid \theta_3 - \theta_4 \mid < 0.06$ rad (for all target positions).
- $60^0 < \theta_{cm} < 120^0$ (for all target positions).

The calculations include all the effects discussed in the Chapters 2 and 3 (i.e. ISI/FSI, EMC, CT) and the strength of the SRC defined with $a_2 = 5$.

Figure 16 shows the comparison between the measured transverse p_y distribution and the calculated distribution. The theoretical and experimental distributions are normalized to 1000 at the first bin so only the difference in shape between them is relevant. They are for the combined 5.9 GeV/c and 7.5 GeV/c data and the upstream target ($\alpha = 0.79 \pm 0.05$). See chapter 4 for the detailed procedure of combining the 5.9 GeV/c and 7.5 GeV/c data sets. We followed the same procedure in the calculations. Figure 17 shows the similar to Figure 16 comparison for the kinematics of the middle stream target ($\alpha = 0.87 \pm 0.05$).

The calculations presented in Figure 16 and 17 overestimate the data at the transverse missing momenta above 0.2 GeV/c. There are several reasons for such a discrepancy. First, one should notice that the tail of the distribution above $p_y = 200 MeV/c$ is only 10% of the peak value at $p_y = 0$. Since calculation and the data are normalized at the maximum, even small discrepancy between calculation and the data at $p_y = 0$ will reproduce a large discrepancy at large values of p_y.

Next, this discrepancy may be the indication of the limit of applicability of the probabilistic approximation of ISI/FSI. In this approximation we neglected the interference terms which may contribute at large values of transverse momenta. Indeed as the complete calculation of $d(p, 2p)n$ reaction demonstrated [29] the interference terms are not negligible at $p_t \geq 150 - 200 MeV/c$ and their contribution tends to diminish the overall cross section.

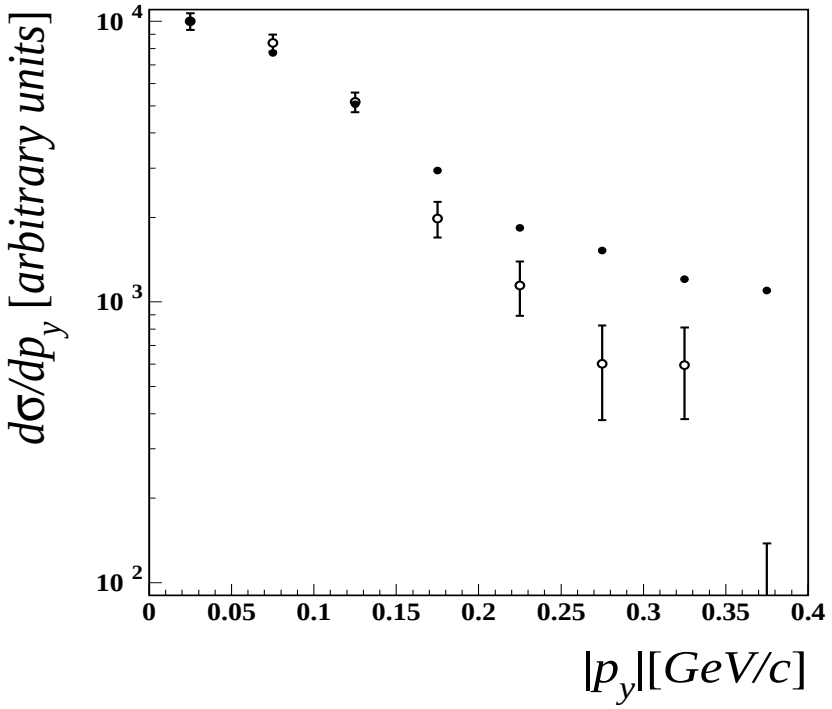

FIG. 17. A comparison of calculated (•) and experimental (○) p_y distributions for combined 5.9 GeV/c and 7.5 GeV/c energies. The kinematics of the middle stream target with $0.82 < \alpha < 0.92$ is used (see text for details).

Another reason for the discrepancy may be the fact that within the eikonal approximation, starting at transverse missing momenta ($\geq 150 - 200 MeV/c$) the ISI and FSI are dominated by incoherent elastic rescattering which enhance the cross section of the nuclear reaction (see for the details Ref. [44]). It was observed in Refs. [45,46] that incoherent elastic rescatterings are much more sensitive to the CT phenomena then the nuclear absorption is. The qualitative reason is that the absorption is proportional to the total cross section of PLC-N interaction, $\sigma^{tot}_{PLC,N}$, while incoherent elastic rescattering is proportional to $(\sigma^{tot}_{PLC,N})^2$. Thus the overestimate of the calculation may indicate that the onset of CT is stronger than it is modeled in the calculations (see Section II). Note that a noticeable ($\sim 20\%$) change in the strength of the incoherent elastic rescattering will result only $\sim 5\%$ change of the absorption thus such a modification of the size of the CT effect will still maintain the agreement of the calculation with the transparency data of Ref. [31].

Ending the above discussion we can only conclude that the strength of the high transverse momentum distributions is generated by ISI/FSI. However both improved theoretical calculation of ISI/FSI and the better experimental resolution are needed for understanding the details of the dynamics behind the strength of high transverse momentum distributions.

VI. SUMMARY

We present the theoretical analysis of the first published data on the high momentum transfer quasielastic $C(p, 2p)X$ reaction.

First, we outline the light cone plane wave impulse approximation, in which the high momentum component of the nuclear wave function is treated within a two-nucleon short range correlation model. Within the same model it was predicted in Ref. [11] that the α-distribution of the $A(p, 2p)X$ cross section will be shifted to the smaller values of α thereby enhancing the contribution from SRC. We further develop the SRC model taking into account the medium modification of the bound nucleon as well as initial and final state reinteractions of the incoming and two outgoing protons in the nuclear medium, combined with the color transparency effects.

For nuclear medium modification we demonstrated that within the color screening model, which describes reasonably the available electroproduction data, the strength of the SRC is not obscured. Furthermore we demonstrated that in the high energy regime the α-distribution of the bound proton is practically unaltered by ISI/FSI. As a result the α-distribution of the $C(p, 2p)X$ cross section reflects the genuine distribution of the bound proton in the nucleus. We also showed that the transverse missing momentum distribution is strongly sensitive to the dynamics of initial and final state reinteractions, and discussed its potential use to study the effects related to the color transparency phenomena.

In addition to the α and p_t distributions we discussed the dependence of the cross section on the total longitudinal momentum of the two outgoing protons. It indicates the existence of a nuclear "boosting" effect, in which the longitudinal momentum of the two outgoing protons is larger than the momentum of the incoming proton. This result is in qualitative agreement with the new data recently obtained at EVA [32].

After briefly describing the experiment we proceed with comparison of the theoretical calculations with the data. The comparison demonstrates that the theoretical expectation of the α shift, based on scaling in hard elastic scattering off a bound nucleon in the nucleus,

is correct. The physical meaning of these shifts is that hard quasi elastic pp scattering is sensitive to the high momentum components of the nuclear wave function. One observes that a momentum tail in the nuclear wave function that is needed to explain the data is significantly larger than what is expected from the mean field approximation. The value of the two nucleon SRC strength needed to describe the data is in agreement with the SRC strength obtained from electronuclear reactions. The analysis of the transverse missing momentum distribution shows that it is very sensitive to the mechanism of ISI/FSI and both improved calculations and the data are needed for understanding the details of the dynamics that generates the high transverse momentum strength. Thus the studies of the transverse-momentum distribution may emerge as an additional tool for study the color transparency phenomena.

ACKNOWLEDGEMENTS

Part of the data related to p_y distribution have not been published before. We would like to acknowledge the EVA collaboration allowing us to present them in this paper. The authors are thankful to the EVA collaboration, especially to the spokespersons: S. Heppelmann and A. Carroll for very useful discussions. Special thanks to Y. Mardor for providing the details of her analysis of the experimental data.

M. Sargsian gratefully acknowledges a contract from Jefferson Lab under which this work was done. The Thomas Jefferson National Accelerator Facility (Jefferson Lab) is operated by the Southeastern Universities Research Association (SURA) under DOE contract DE-AC05-84ER40150. This work is supported also by DOE grants under contract DE-FG02-01ER-41172 and DE-FG02-93ER-40771 as well as by the U.S. - Israel Binational Science foundation and the Israel Science Foundation founded by the Israel Academy of Sciences and Humanities.

REFERENCES

[1] S.J. Brodsky and G.R. Farrar, Phys. Rev. Lett. **31**, 1153 (1973); Phys. Rev. **D11**, 1309 (1975); V. Matveev, R.M. Muradyan and A.N. Tavkhelidze, Lett. Nuovo Cimento **7**, 719 (1973).

[2] N. Isgur and C.H. Llewellyn Smith, Phys. Rev. Lett. **52**, (1984) 1080; Phys.Lett. **B217**, 535 (1989).

[3] A. Radyushkin, Acta Phys. Pol. **B15**, 403 (1984).

[4] S. J. Brodsky, C. E. Carlson and H. J. Lipkin, Phys. Rev. **D20**, 2278 (1979).

[5] G. R. Farrar, S. Gottlieb, D. Sivers and G. H. Thomas, Phys. Rev. **D20**, 202 (1979).

[6] G. P. Ramsey and D. Sivers, Phys. Rev. **D52**, 116 (1995).

[7] P. Landshoff, Phys. Rev. **D10**, 1024 (1974); P. Landshoff and D. Pritchard, Z.Phys. **C6**, 69 (1980).

[8] J. Botts and G. Sterman, Nucl. Phys. **B325**, 62 (1989).

[9] C. Bourrely and J. Soffer, Phys. Rev. **D35**, 145 (1987).

[10] L.L. Frankfurt and M.I. Strikman, Phys. Rep. **160**, 235 (1988).

[11] G. R. Farrar, H. Liu, L. L. Frankfurt, and M. I. Strikman Phys. Rev. Lett. **62**, 1095 (1989).

[12] Y.Mardor *et al.*, Phys. Lett. B437(1998) 257.

[13] R. Feynman, *Photon - Hadron Interactions*, W.A. Benjamin Inc. 1972.

[14] L.L. Frankfurt and M.I. Strikman, Phys. Rep. **76**, 214 (1981).

[15] L. L. Frankfurt, M. I. Strikman, D. B. Day and M. Sargsian, Phys. Rev. **C48**, 2451 (1993).

[16] C. Ciofi degli Atti, S. Simula, L. L. Frankfurt and M. I. Strikman, Phys. Rev. **C44**, 7 (1991).

[17] S. J. Brodsky and G. F. de Teramond, Phys. Rev. Lett. **60**, 1924 (1988).

[18] D. Sivers, S.J. Brodsky and R. Blankenbecler, Phys. Rep. **23**, 1 (1976).

[19] L. Frankfurt, E. Piasetsky, M. Sargsian and M. Strikman, Phys. Rev. **C51**, 890 (1995).

[20] J.J. Aubert *et al.* (EM Collaboration), Phys. Lett. B **123**, 275 (1983).

[21] L. L. Frankfurt and M. I. Strikman, Nucl. Phys. **B250** (1985) 143.

[22] M. R. Frank, B. K. Jennings and G. A. Miller, Phys. Rev. C **54**, 920 (1996).

[23] L. L. Frankfurt, M. I. Strikman and M. B. Zhalov, Phys. Rev. **C50**, 2189 (1994).

[24] R.L. Jaffe, F.E. Close, R.G. Roberts and G.G. Ross: Phys. Lett. **B134**, 449 (1984).

[25] W. Melnitchouk, M. Sargsian and M. I. Strikman, Z. Phys. A **359**, 99 (1997).

[26] L. Frankfurt, G. A. Miller and M. Strikman, Phys. Rev. Lett. **68**, 17 (1992).

[27] I. Mardor, Y. Mardor, E. Piasetzky, J. Alster and M. M. Sargsian, Phys. Rev. C **46**, 761 (1992)

[28] L. L. Frankfurt, M. M. Sargsian and M. I. Strikman, Phys. Rev. C **56**, 1124 (1997).

[29] L. L. Frankfurt, E. Piasetzky, M. M. Sargsian and M. I. Strikman, Phys. Rev. C **56**, 2752 (1997).

[30] M. M. Sargsian, Int. J. Mod. Phys. E **10**, 405 (2001).

[31] A. S. Carroll *et al.*, Phys. Rev. Lett. **61**, 1698 (1988).

[32] A. Leksanov *et al.*, Phys. Rev. Lett. **87**, 21230 (2001).

[33] G. R. Farrar, H. Liu, L. L. Frankfurt and M. I. Strikman, Phys. Rev. Lett. **61**, 686 (1988).

[34] L. Frankfurt, G. A. Miller and M. Strikman, Comments Nucl. Part. Phys. **21**, 1 (1992).

[35] N. Makins *et al.,(NE18 collaboration)* Phys. Rev. Lett. **72**, 1986 (1994).
[36] Y. Mardor *et al.* Phys. Rev. Lett. **81**, 5085 (1998).
[37] J. P. Ralston and B. Pire, Phys. Rev. Lett. **61**, 1823 (1988).
[38] B. K. Jennings and G. A. Miller, Phys. Lett. B **318**, 7 (1993).
[39] J.Y.Wu *et al.* , Nuclear Instruments and Methods A 349 (1994) 183.
[40] M.A.Shupe *et al. EVA, a solenoidal detector for large angle exclusive reactions: Phase I - determining color transparency to 22 GeV/c.* Experiment E850 Proposal to Brookhaven National Laboratory, 1988 (unpublished).
[41] *Measurement of the dependence of the $C(p, 2p)$ cross section on the transverse component of the spectral momentum*, S.Durrant, PhD thesis, Pennsylvania State University, 1994 (unpublished).
[42] *Quasi-Elastic Hadronic Scattering at Large Momentum Transfer*, Y.Mardor, PhD thesis, Tel Aviv University, 1997 (unpublished).
[43] K. Garrow *et al.*, arXiv:hep-ex/0109027, (2001).
[44] D.R. Yennie, *in Hadronic Interactions of Electrons and Photons*, edited by J. Cummings and D. Osborn (Academic, New York, 1971), p.321.
[45] K.Sh. Egiyan, L.L. Frankfurt, W. Greenberg, G.A. Miller, M.M. Sargsian and M.I. Strikman, Nucl. Phys. A **580**, 365 (1994).
[46] L.L. Frankfurt, G.A. Miller, W. Greenberg, M.M. Sargsian and M.I. Strikman, Z. Phys. A **352**, 97 (1995).